

# The Monod-Wyman-Changeux allosteric model accounts for the quaternary transition dynamics in wild type and a recombinant mutant human hemoglobin

Matteo Levantino<sup>a,1</sup>, Alessandro Spilotros<sup>a,1</sup>, Marco Cammarata<sup>b</sup>, Giorgio Schirò<sup>a</sup>, Chiara Ardiccioni<sup>c</sup>, Beatrice Vallone<sup>c</sup>, Maurizio Brunori<sup>c,2</sup>, and Antonio Cupane<sup>a</sup>

<sup>a</sup>Department of Physics, University of Palermo, Via Archirafi 36, I-90123 Palermo, Italy; <sup>b</sup>Institut de Physique de Rennes, Centre National de la Recherche Scientifique, 263 Avenue Général Leclerc, 35042 Rennes, France; and <sup>c</sup>Department of Biochemical Sciences, and Istituto Pasteur-Fondazione Cenci Bolognetti, Sapienza—University of Rome, Piazzale Aldo Moro 5, I-00185 Rome, Italy

Edited by Martin Karplus, Harvard University, Cambridge, MA, and approved August 3, 2012 (received for review April 17, 2012)

The acknowledged success of the Monod-Wyman-Changeux (MWC) allosteric model stems from its efficacy in accounting for the functional behavior of many complex proteins starting with hemoglobin (the paradigmatic case) and extending to channels and receptors. The kinetic aspects of the allosteric model, however, have been often neglected, with the exception of hemoglobin and a few other proteins where conformational relaxations can be triggered by a short and intense laser pulse, and monitored by time-resolved optical spectroscopy. Only recently the application of time-resolved wide-angle X-ray scattering (TR-WAXS), a direct structurally sensitive technique, unveiled the time scale of hemoglobin quaternary structural transition. In order to test the generality of the MWC kinetic model, we carried out a TR-WAXS investigation in parallel on adult human hemoglobin and on a recombinant protein (HbYQ) carrying two mutations at the active site [Leu(B10)Tyr and His(E7)Gln]. HbYQ seemed an ideal test because, although exhibiting allosteric properties, its kinetic and structural properties are different from adult human hemoglobin. The structural dynamics of HbYQ unveiled by TR-WAXS can be quantitatively accounted for by the MWC kinetic model. Interestingly, the main structural change associated with the R–T allosteric transition (i.e., the relative rotation and translation of the dimers) is approximately 10-fold slower in HbYQ, and the drop in the allosteric transition rate with ligand saturation is steeper. Our results extend the general validity of the MWC kinetic model and reveal peculiar thermodynamic properties of HbYQ. A possible structural interpretation of the characteristic kinetic behavior of HbYQ is also discussed.

time-resolved X-ray scattering | protein conformational changes | cooperativity | flash photolysis

Ever since the publication of the Monod-Wyman-Changeux paper on allostery (1), hemoglobin (Hb) has been considered the prototype of an allosteric protein; the molecular basis of positive cooperativity in O<sub>2</sub> binding involving a ligand-linked shift between two different quaternary states. The dynamics of ligand rebinding and of the tertiary and quaternary allosteric changes of tetrameric human Hb have been investigated, by-and-large, using transient spectroscopy in the picosecond to millisecond time range, following laser-induced photolysis of the ligand-heme iron bond. Starting with the carbon monoxide adduct HbCO in the allosteric quaternary state called R<sub>4</sub>, complete photolysis yields the unliganded R<sub>0</sub> state; the destiny of this photoproduct is a complex time-dependent process involving competing events such as ligand rebinding and (tertiary and quaternary) conformational decays. Changes in the optical and resonance Raman spectra of the different states have provided, over the last four decades, a quantitative estimate of the rates of the competing events (2–5). For a review on time-resolved optical absorption (TR-OA) data describing conformational decays as well as rebinding in the dark of a ligand escaped into the solvent (bimolecular) or trapped within the protein matrix (geminate), see Eaton et al. (6).

It is generally accepted that tertiary structural changes within the  $\alpha$  and  $\beta$  subunits occur in the nanosecond time regime and follow a complex time course. The much larger structural changes of the quaternary allosteric transition (involving shifts in the inter-subunit contacts and relative motions of the two symmetric dimers  $\alpha_1\beta_1/\alpha_2\beta_2$ ) occur in the microsecond time range; the single time constant estimated from optical changes of the deoxy photoproduct is about 20  $\mu$ s for human HbA at neutral pH and 20 °C (2, 3, 6, 7). The dynamics of the structural changes followed by ultraviolet resonance Raman (UVRR) spectroscopy after laser photolysis showed, however, the quaternary conformational transition involving contacts at the  $\alpha_1\beta_2$  and  $\alpha_2\beta_1$  interfaces (8, 9) to be more complex. Since the UVRR spectra of Trp37 $\beta$  and Tyr42 $\alpha$  are distinct, it was possible to show that upon population of the T state (i) Trp37 $\beta$  forms a H-bond with Asp94 $\alpha$  at the “hinge” region of the  $\alpha_1\beta_2$  interface, and (ii) Tyr42 $\alpha$  forms an H-bond with Asp99 $\beta$  at the switch region (5, 10), the former T state contact being established in 2  $\mu$ s while the latter forms in 20  $\mu$ s. A similar 2  $\mu$ s phase has also been detected by time-resolved magnetic circular dichroism associated with Trp (11).

All spectroscopic probes, valuable as they are, provide limited information on the global structure of the protein and therefore on the dynamic profile of the major allosteric transition. However recently Cammarata et al. (12, 13) published the first experiments using time-resolved wide-angle X-ray scattering (TR-WAXS) on Hb and unveiled the protein motions related to the tertiary and quaternary conformational changes. Following laser photodissociation of CO, the early (147 ns) post-photolysis signal evolved toward the well defined deoxyHb vs. HbCO scattering difference pattern in about 2  $\mu$ s. This estimate implies that dimer rotation—the largest structural change in the R–T allosteric transition—is much faster than 20  $\mu$ s, the time constant detected by optical spectroscopy (2, 3). Quite recently Fischer et al. (14) published a computational analysis of Hb dynamics which revealed distinct tertiary and quaternary conformational events; in particular, they reported two sequential quaternary changes (called Q<sub>1</sub> and Q<sub>2</sub>), which they assumed to be consistent with the time constants at 2  $\mu$ s (for Q<sub>2</sub>) and 20  $\mu$ s (for Q<sub>1</sub>) reported by Balakrishnan et al. (10).

We have repeated the TR-WAXS experiment on wild-type human HbA employing a different laser pulse, and in parallel analyzed a recombinant mutant called HbYQ (15, 16) with the

Author contributions: M.L., M.C., B.V., M.B., and A.C. designed research; M.L., A.S., M.C., G.S., C.A., B.V., and A.C. performed research; B.V. contributed new reagents/analytic tools; A.S. and G.S. contributed to the manuscript design; M.L., A.S., and A.C. analyzed data; and M.L., B.V., M.B., and A.C. wrote the paper.

The authors declare no conflict of interest.

This article is a PNAS Direct Submission.

<sup>1</sup>M.L. and A.S. contributed equally to this work.

<sup>2</sup>To whom correspondence should be addressed. E-mail: maurizio.brunori@uniroma1.it.

This article contains supporting information online at [www.pnas.org/lookup/suppl/doi:10.1073/pnas.1205809109/-DCSupplemental](http://www.pnas.org/lookup/suppl/doi:10.1073/pnas.1205809109/-DCSupplemental).

$\alpha$  and  $\beta$  chains containing two mutations in the distal heme pocket—i.e., His(E7)Gln and Leu(B10)Tyr—which was characterized (15–17) by crystallography, transient spectroscopy, and ligand binding experiments. The main motivation to undertake the TR-WAXS experiment on HbYQ was to test the general validity of this approach to follow the time evolution of the global structure of the protein in solution. HbYQ seemed a promising case because this variant undergoes a ligand-linked allosteric transition and binds  $O_2$  cooperatively, albeit with much reduced affinity and a smaller Hill's coefficient ( $n = 1.8$  vs. 2.9 for HbA). The structure of the deoxy  $T_0$ -state, identical to that of HbA, when exposed to CO yields an intermediate with the ligand bound only at the  $\beta$  chains. Assuming  $L_0$  (the population ratio of the  $T_0$  to  $R_0$  states) to be the same for HbA and HbYQ,  $O_2$  binding was fitted to the MWC model with a switch-over point  $\geq 3$ ; this parameter, which indicates the average number of bound ligands at which the two quaternary states are equally populated, is reported to be about 2 for HbA (2, 9). Relative to HbA, in HbYQ the CO bimolecular rate constant is much smaller and no significant geminate rebinding is detected because of steric hindrance by TyrB10 (as seen for a similar mutant of sperm whale myoglobin) (18, 19). This is of considerable advantage because (i) essentially no CO rebinding will take place in the nanosecond time scale, and (ii) a large fraction of tetramers will undergo the R–T transition even with a 3-ns-long photolysis pulse, at variance with HbA. The results reported below are very satisfactory insofar as the TR-WAXS data on HbA and HbYQ can be fitted within the canonical kinetic allosteric model in spite of the significant differences; thus the new data support the general validity of the model and of the experimental approach alike. Unexpectedly, however, the time constant of the  $R_0 \rightarrow T_0$  quaternary transition for HbYQ is 12.4  $\mu$ s, and therefore clearly slower than the value of 1–2  $\mu$ s previously reported for HbA by Cammarata et al. (12, 13). Based on the crystallographic data of Miele et al. (15, 17), we propose a possible structural mechanism for the slow down of the quaternary allosteric transition observed in HbYQ.

## Results

**Time-Resolved Scattering.** In order to track and compare the structural dynamics of HbA and HbYQ, we have collected TR-WAXS

difference patterns,  $\Delta S(q)$ , of both proteins at several time delays after photolysis (Fig. 1). The overall shape of the HbYQ difference patterns is analogous to that of HbA, indicating that the structural intermediates involved in the R–T transition of the two variants are similar. Nevertheless, differences in the time evolution of the patterns are evident. In the nanosecond time scale, TR-WAXS patterns (due to tertiary structural changes) are similar both in shape and amplitude. Note that the 3.16 ns and 316 ns patterns have different shapes, both in the case of HbA and HbYQ, reflecting the complex nature of the tertiary transition, as documented for myoglobin (18, 20). The 100  $\mu$ s TR-WAXS patterns (due to quaternary structural changes) (12, 13) are very similar in shape, but the amplitude of the HbA signal is significantly smaller; at longer time delays (when CO bimolecular rebinding dominates), the HbA signal decays much more rapidly, becoming negligible at 100 ms. The clear cut amplitude difference of the 100  $\mu$ s TR-WAXS patterns reveals a larger fraction of tetramers undergoing the R–T transition in HbYQ, as expected since geminate rebinding is essentially absent (17). Moreover, the observed signal evolution in the microsecond time scale agrees with a much smaller CO bimolecular rebinding rate to T state HbYQ (15), consistently with the 3D structure (*SI Discussion* and Figs. S1–S3).

As reported by Cammarata et al. (13), the peak at about  $0.19 \text{ \AA}^{-1}$  in the TR-WAXS difference patterns can be used to monitor the kinetics of the overall structural changes of the globin after photolysis. Fig. 24 reports the time evolution of the amplitude of this peak for both proteins: the signal initially increases due to both tertiary and quaternary structural changes, then reaches a maximum mostly determined by the number of tetramers undergoing the R–T transition, and finally decreases to zero due to bimolecular rebinding of CO to deoxyHb, leading back to fully saturated R state. The number of Hb molecules undergoing the R–T transition (as judged by the approximate maximum of the  $0.19 \text{ \AA}^{-1}$  peak) is greater in HbYQ than in HbA. In view of the various physical processes (geminate and bimolecular rebinding, tertiary and quaternary relaxations) underlying the observed signal time evolution, it is not easy to estimate quantitatively the R–T transition rates for the two variants from the data reported in Fig. 24. The different population of R state Hb tetramers partially bound to CO due to geminate rebinding, which is

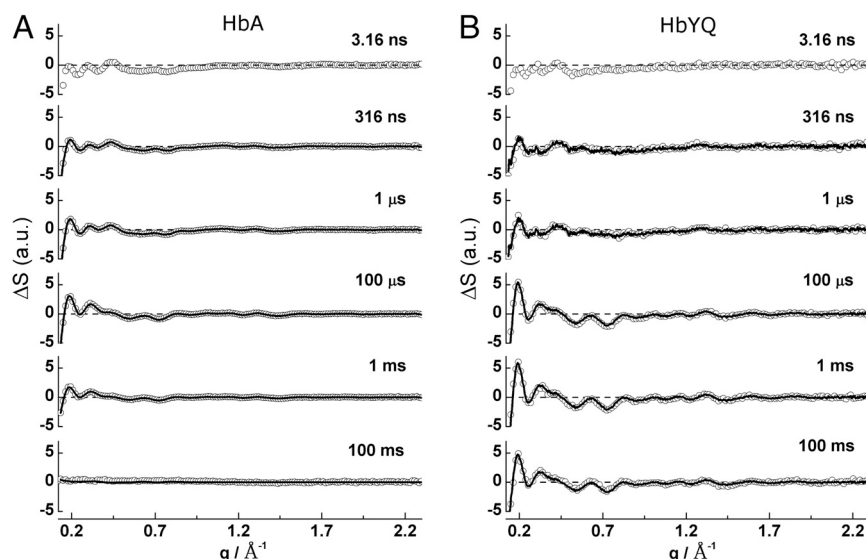


**Fig. 1.** TR-WAXS difference patterns of HbA (A) and HbYQ (B) measured at different time delays from a 3-ns-long photolysis pulse. Continuous lines are fitting curves obtained from a global analysis of the experimental patterns at time delays longer than 250 ns as described in the text. A fast local structural change is detected at 3.16 ns in both HbA and HbYQ. At 100  $\mu$ s the typical pattern assigned to the  $\alpha\beta$  dimers relative rotation and translation is observed (12, 13); its amplitude is larger for HbYQ than for HbA due to the large difference in geminate rebinding. At 100 ms, while HbA has already recombined with CO, HbYQ is still mostly in the deoxy state due to the smaller bimolecular rebinding rate.

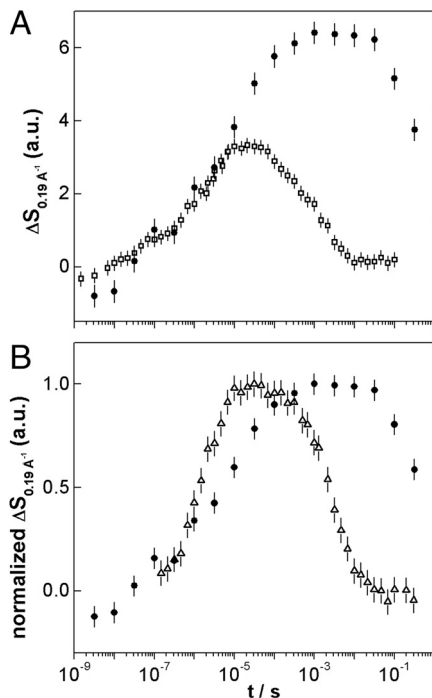


**Fig. 2.** (A) Time dependence of the TR-WAXS signal at  $-0.19 \text{ \AA}^{-1}$ . For HbA (open squares) the maximum value of the signal is smaller than for HbYQ (closed circles); both sets of data have been obtained using a 3-ns-long photolysis pulse. (B) HbYQ signal obtained with a 3-ns-long photolysis pulse (closed circles) compared with the HbA signal obtained with a 230-ns photolysis pulse (open triangles, data from ref. 13); both signals have been normalized to their maximum. Error bars have been estimated from the noise of the difference patterns.

relevant for HbA but negligible for HbYQ, is crucial because partially bound R state molecules relax to the corresponding T states more slowly than  $R_0$  (2). A more appropriate comparison of raw data time evolution demands a similar initial population of  $R_i$  species; this was obtained in a previous experiment on HbA using a 230-ns photolysis pulse (13), long enough to rephotolyze geminate states, thus pumping the system towards  $R_0$  (2, 3, 6). Once the initial distribution of the  $R_i$  populations is quite similar, the comparison highlights that the R–T transition of HbYQ is significantly slower than that of HbA (Fig. 2B).

**MWC Allosteric Kinetic Model.** In order to estimate the kinetic parameters characterizing the dynamics of the two variants of Hb, the TR-WAXS data were analyzed with a kinetic model describing the various physical processes occurring after photolysis. However, developing a kinetic model including both faster (geminate rebinding and tertiary relaxations) and slower (quaternary relaxations and bimolecular rebinding) processes would require the introduction of too many different species (21, 22), and the number of kinetic parameters would exceed the accuracy of present day TR-WAXS data. A great simplification is obtained if only data at time delays longer than about 250 ns are considered given that both geminate rebinding and tertiary relaxations are expected to be over (10, 23). This enables the use of the canonical MWC kinetic model previously employed to analyze the dynamics of the allosteric transition of HbA as followed by TR-OA (2, 3), and recently applied to TR-WAXS data (12, 13) (*Materials and Methods*, Fig. S4). The entire data set has been reconstructed as a linear combination of a  $\Delta S_{R\text{-like}}(q)$  basis pattern corresponding to unrelaxed R state Hb, and a  $\Delta S_{T\text{-like}}(q)$  pattern corresponding to T state Hb,

$$\Delta S(q, t) = R\text{-like}(t)\Delta S_{R\text{-like}}(q) + T\text{-like}(t)\Delta S_{T\text{-like}}(q), \quad [1]$$

where R-like(t) and T-like(t) are weighted sums of the  $R_i(t)$  and  $T_i(t)$  populations, respectively. A fit of the experimental data allows a reliable determination of basis patterns and kinetic parameters such as the  $R_0$ – $T_0$  transition rate constant ( $k_0$ ) and the fraction of deoxy-hemes at 250 ns from photolysis ( $N_0$ ). Fig. 3 A and B reports the basis patterns obtained for HbA and HbYQ, respectively; the corresponding R-like(t) and T-like(t) populations are shown in Fig. 3 C and D and best fit values of kinetic parameters are given in Table 1. It may be seen that in spite of the mutations and their effect on the geminate rebinding yield, the basis patterns obtained for HbA and HbYQ are very similar, supporting the conclusion that the structural changes involved in the R–T transition are essentially the same for the two Hb variants, in agreement with crystallographic data on deoxygenated T state HbYQ (15, 17). The time course of the intermediate species populations has a similar overall shape (Fig. 3 C and D). At 250 ns the fraction of Hb tetramers in the R state is quite different in the two variants (81% vs. 52%) because of the large difference in geminate rebinding extent. Thereafter the R-like population decreases due to quaternary transition and bimolecular rebinding. In turn, the T-like population initially increases due to the  $R_i$ – $T_i$  quaternary transition and finally disappears due to bimolecular rebinding of CO.

In the case of HbA the kinetic parameters resulting from the new data obtained using a 3-ns laser pulse are in good agreement with those previously obtained (13) using a 230-ns laser pulse at three different protein concentrations (0.25, 0.5, and 1 mM). As already outlined, in the latter experiments the longer laser pulse rephotolyzed the partially bound R states populated via geminate rebinding, increasing the fraction of deoxy-hemes at 250 ns from photolysis (72–80% vs. about 50%). The  $R_0$ – $T_0$  transition time (i.e.,  $\tau_0 = 1/k_0$ ) is slightly shorter (1.0  $\mu\text{s}$  vs. 1.2–1.9  $\mu\text{s}$ ) and the parameter  $s$  (2, 3), which defines the increase of the quaternary transition time as the ligands bound to R increase from 1 to 4 (e.g.,  $\tau_1 = \tau_0 \times s$  in the case of the  $R_1$ – $T_1$  transition), is smaller than that previously reported (9 vs. 14–26). Note that, in view of the much higher fraction of tetramers that undergo the  $R_1$ – $T_1$  transition in the present experiment, the new  $s$  value is better determined than the previous one. The value of  $L_0 = 1.7 \times 10^4$  obtained from the present experiment is similar to that reported by Cammarata et al. (13), although smaller than that generally accepted for HbA (see *Structural Interpretation* for further comments). Finally, the value  $1.4 \times 10^{-3}$  obtained for the affinity ratio  $c$  is within the range of values previously obtained (i.e.,  $0.8$ – $6.1 \times 10^{-3}$ ), and close to that obtained from the equilibrium CO binding data of Perrella et al. (24, 25). In a nutshell, present analysis confirms that in HbA the largest structural rearrangement associated to the R–T transition (i.e., the relative  $\alpha\beta$  dimers rotation and translation) is faster than what has been obtained by TR-OA data (2, 3, 23, 26), though consistent with the faster step seen by UVRR and assigned to the relaxation of Trp37 $\beta$  (5, 10).

In the case of HbYQ, the kinetic parameters (Table 1) show significant differences with respect to HbA. In agreement with the lack of geminate rebinding, the  $N_0$  value is higher than that obtained for HbA using a 3-ns laser pulse and falls within the range obtained with the latter protein using a 230-ns photolysis pulse. The  $R_0$ – $T_0$  transition time, however, is significantly longer than that of HbA (12.4  $\mu\text{s}$  vs. 1.0  $\mu\text{s}$ ), and the  $s$  value is higher. Although no equilibrium CO binding data is available for HbYQ, the  $c$  value of 0.021 is not inconsistent with that calculated from the  $O_2$  binding data on the same mutant (15) assuming  $L_0 = 2 \times 10^4$ .

## Discussion

We have documented above that in the double mutant HbYQ, the  $R_0$ – $T_0$  transition, which involves the relative rotation and translation of the two  $\alpha\beta$  dimers, is about an order of magnitude slower than in HbA, while the overall structural states detected by

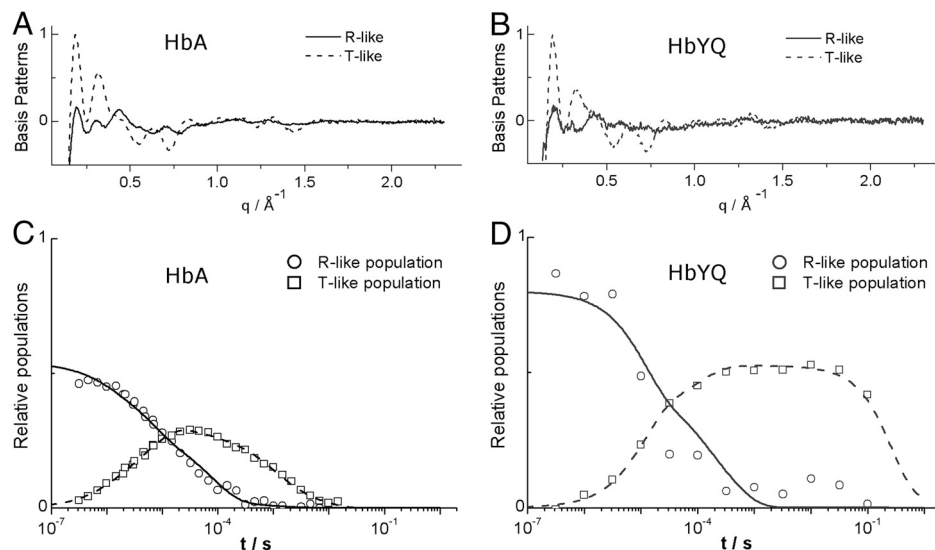


**Fig. 3.** Results of the global analysis of TR-WAXS patterns according to the MWC allosteric kinetic model for HbA and HbYQ based on data obtained with a 3-ns laser pulse for both proteins. *Top*s: normalized basis patterns obtained for HbA (A) and HbYQ (B). *Bottom*s: relative R-like and T-like populations for HbA (C) and HbYQ (D) as obtained from the decomposition of experimental patterns in terms of a linear combination of the basis patterns reported in A and B (symbols), and from the kinetic model (lines).

TR-WAXS are fairly similar. We conclude that the two mutations at the active site [His(E7)Gln and Leu(B10)Tyr] not only abolish CO geminate yield, reduce the rate of bimolecular rebinding, and cause  $\alpha\beta$  chain heterogeneity, but also increase the activation barrier for the large conformational transition basic to the Hb allosteric behavior. This feature would not have been discovered without TR-WAXS that, being directly sensitive to the overall structure of the protein, is the most suitable technique to follow the dynamics of the overall conformational changes of a protein in solution.

**Thermodynamic Properties of the R–T Transition State.** Relevant information on the activation free energy for the  $R_i$ – $T_i$  dimers rotation and translation ( $\Delta G_i^\ddagger$ ) can be obtained following Eaton and coworkers (23) who applied the linear free energy relationship between the activation energy of the  $R_i$ – $T_i$  transition and the equilibrium free energy difference between  $R_i$  and  $T_i$  states:

$$\Delta G_i^\ddagger = \alpha \Delta G_i + \text{constant.} \quad [2]$$

The parameter  $\alpha$ , with values between 0 and 1, may be interpreted as a measure of the thermodynamic properties of the transition state, that for  $\alpha = 0$  would be R-like and conversely for  $\alpha = 1$  would be T-like. The allosteric kinetic model used to fit our TR-WAXS data implicitly assumes the validity of Eq. 2 with  $\alpha = -\log(s)/\log(c)$ ; the values reported in Table 1 yield  $\alpha = 0.33$  and 0.81 for HbA and HbYQ, respectively. In the case of HbA, the difference between our estimate and the value of  $\alpha = 0.17$  determined by TR-OA data (23) may be traced to the proposed stepwise character of the R–T allosteric transition (10, 14, 26). Following this idea, Cammarata et al. (13) proposed that TR-WAXS essentially monitors a first step of the R–T transition of

HbA (namely the  $\alpha\beta$  dimers rotation and translation), while TR-OA monitors a second slower step associated with a more localized reorganization around the active site; accordingly, the transition states explored by TR-WAXS and TR-OA spectroscopy are not the same (Fig. S5). This interpretation is consistent with recent conjugate peak refinement calculations (14) presenting a stepwise allosteric transition that, seen along the R to T pathway, consists of a larger quaternary transition ( $Q_2$  in their terminology) followed by a smaller quaternary step ( $Q_1$ ) coupled to a residual tertiary change. In light of the above scenario, the value  $\alpha = 0.33$  obtained for HbA by TR-WAXS implies that the transition state associated to the  $\alpha\beta$  dimers rotation has thermodynamic properties closer to the R state than to the T state; while in the case of HbYQ, the transition state has thermodynamic properties considerably more similar to those of the T state, given that  $\alpha = 0.81$ . It is not easy to propose a structural interpretation for this observation since it may involve differences in the shape of the free energy profile along the reaction coordinate, as suggested by Edelstein and Changeux (27). Moreover, in view of the complexity of the R–T transition, we cannot exclude that the higher value of  $\alpha$  observed for HbYQ simply reflects the merging of the two quaternary steps in the mutant.

**Structural Interpretation.** Miele et al. (15, 17) demonstrated that HbYQ in solution undergoes a ligand-linked structural change recalling that of HbA (8, 9, 28). The 3D structure of deoxy T state HbYQ is identical to that of T state HbA to high resolution, apart for the two mutations introduced in the distal heme pocket. To fit the  $O_2$  binding data, Miele et al. (15) boldly assumed that  $L_0 = 1.4 \times 10^6$  would be the same for both proteins. Likewise the values of  $L_0$  obtained from the fit of the TR-WAXS data (Table 1), though much smaller ( $L_0 = 1.7$  or  $2.0 \times 10^4$ ), are pretty much

**Table 1.** Kinetic parameters obtained by the fitting procedure described in the text

Sample	$N_0$	$\tau_0 = 1/k_0$ ( $\mu\text{s}$ )	$s$	$L_0 \times 10^{-3}$	$c \times 10^3$	${}^Rk_{\text{on}}^*$ ( $\mu\text{M}^{-1} \text{s}^{-1}$ )	${}^Tk_{\text{on}}^*$ ( $\text{mM}^{-1} \text{s}^{-1}$ )
HbYQ	0.81 ( $\pm 0.01$ )	12.4 ( $\pm 0.6$ )	23 ( $\pm 1$ )	20 ( $\pm 8$ )	21 ( $\pm 8$ )	1	0.75
HbA	0.518 ( $\pm 0.004$ )	0.96 ( $\pm 0.05$ )	8.6 ( $\pm 0.4$ )	17 ( $\pm 2$ )	1.4 ( $\pm 0.1$ )	5	32.5

\*Parameters  ${}^Rk_{\text{on}}$  and  ${}^Tk_{\text{on}}$  have been fixed to values derived from partial photolysis and stopped-flow experiments, respectively (17).

the same for the two variants; therefore it is unlikely that the slowdown of the  $R_0$ - $T_0$  transition rate observed in HbYQ could be accounted for by a significant stabilization of the  $R_0$  state. Note that, given the stepwise character of the Hb quaternary transition, the overall  $L_0$  value estimated by equilibrium  $O_2$  binding data may not be directly comparable to the value obtained by TR-WAXS, which is sensitive to the fastest and structurally most prominent kinetic step.

Can we identify in HbYQ some perturbation of the  $\alpha_1\beta_2$  interface correlated to the active site motions and possibly affecting the quaternary transition barrier? The high-resolution crystal structures of deoxy and CO-bound HbA (29) were compared with data available for deoxy T state HbYQ and those of the same crystals exposed to CO, which was found to bind only to the  $\beta$  chains (15–17, 30). We focus in this discussion on two crucial residues—i.e., Trp37(C3) $\beta$  and His97(FG4) $\beta$ —both located at the  $\alpha_1\beta_2$  interface contributed by residues of the C helix and FG corner of the  $\alpha$  and  $\beta$  chains (Fig. 4). Spectroscopic and crystallographic studies have shown that the  $\alpha\beta$  dimers rotation is associated with a rearrangement around Trp37(C3) $\beta$ , located in the so-called “hinge” region. In discussing their conjugate peak refinement calculations, Fischer et al. (14) pointed out that the transition of His97(FG4) $\beta$  gliding over Thr41(C6) $\alpha$  at the switch interface occurred in the main  $Q_2$  phase of the allosteric conformational change. How do the distal side mutations introduced in HbYQ affect the  $\alpha_1\beta_2$  interface, where the quaternary transition is associated to the largest changes?

The prominent feature upon CO binding to the  $\beta$  chains of T state HbYQ is the swinging of Tyr28(B10) $\beta$ , resulting in a contact with Phe42(CD1) $\beta$  that is displaced from the position occupied in HbA (Fig. 4B). This pressure can be transmitted *via* Phe41(C7) $\beta$  to both the hinge residue Trp37(C3) $\beta$  and the switch residue

His97(FG4) $\beta$ . In the  $\alpha$  chains, Pro44(CD2) $\alpha$ , Thr41(C6) $\alpha$  and Thr38(C3) $\alpha$  could also be affected by the motion of Tyr29(B10) $\alpha$  *via* Phe43(CD1) $\alpha$  and Tyr42(C7) $\alpha$ , similarly to that illustrated above for the  $\beta$  subunits (Fig. 4A). This chain of contacts would allow distal tertiary changes to be transmitted from the heme-binding pocket to the hinge and the switch contacts of the  $\alpha_1\beta_2$  interface (Fig. S6). We may therefore hypothesize that in the CO-bound R state of HbYQ, the distal Tyr(B10) push-up, and the subsequent strain transmitted to several other side chains (Fig. 4 A and B) may interfere with the sliding motion of His97(FG4) $\beta$  over Thr41(C6) $\alpha$  in the  $\alpha_1\beta_2$  interface, increasing the energy barrier and slowing down the  $R_0$ - $T_0$  transition.

### Concluding Remarks

The MWC allosteric kinetic model, previously employed to fit the TR-WAXS data on HbA after photolysis with a 230-ns-long laser pulse (12, 13), describes the time evolution of WAXS signals also when a shorter (3-ns-long) laser pulse is used to photolyze the CO adducts of either HbA or of the functionally relevant HbYQ double mutant. Although the model is oversimplified in that it does not explicitly take into account the recently proposed tertiary contributions to the kinetics of the R-T allosteric transition (6), it is able to reproduce the observed kinetics with satisfactory fidelity.

The new set of TR-WAXS experiments on HbA and HbYQ provide a test for the validity of the canonical MWC kinetic model. Indeed, the structural and functional properties of this double mutant of human Hb, with substitutions Leu(B10)  $\rightarrow$  Tyr and His(E7)  $\rightarrow$  Gln on both the  $\alpha$  and  $\beta$  chains, are sufficiently consistent with a cooperative allosteric tetramer to attempt a quantitative comparison with HbA, yet they are different enough to make it a valid test of generality. The unexpected difference between the two variants is the rate of the  $R_0 \rightarrow T_0$  quaternary transition that in HbYQ is slower by a factor of about 10 relative to that previously estimated for HbA (13) and confirmed with the new data reported here. From a comparative analysis of the available 3D structures of HbA and HbYQ we tentatively propose a structural interpretation for a mechanism whereby ligand binding to the mutated site perturbs the critical  $\alpha_1\beta_2$  interface and possibly accounts for an increase in the transition state barrier; this, however, should be taken as a working hypothesis.

In order to reliably test more sophisticated models including two different transition states along the kinetic pathway connecting the R and T states, a combined approach using TR-WAXS, UVRR, and TR-OA on the same sample may be needed. A global fit of data obtained from different techniques could yield well-determined kinetic parameters and constitute a more advanced test for the MWC kinetic model.

### Materials and Methods

**Hb Purification.** HbA was purified from freshly collected human blood with standard techniques (31), while the mutant HbYQ was expressed in *E. coli* and purified as previously reported (15).

**Data Acquisition Protocol.** TR-WAXS patterns were acquired at beamline ID9B of the European Synchrotron Radiation Facility (ESRF) while the machine was running in four-bunch mode. HbCO samples were photolyzed with circularly polarized laser pulses at 532 nm incident on the bottom of the capillary. Delayed quasi-monochromatic X-ray pulses (100 ps, full width at half maximum) penetrated the capillary 0.2 mm above its bottom edge yielding an orthogonal geometry between superimposed X-ray and photolysis pulses. The photolysis energy density at the capillary surface was approximately 2 mJ/mm<sup>2</sup>. Taking into account the bimolecular rebinding rates, X-ray scattering patterns were acquired between 3 ns and 0.1 s (six time delays per decade) for HbA, and between 3 ns and 0.32 s (two time delays per decade) for HbYQ. To dilute any X-ray radiation damage over a large sample volume, the capillary was translated back and forth over a 25-mm range, ensuring that each laser pulse excited adjacent but spatially separated sample volumes. Scattered X-rays were recorded in the forward direction by a sensitive CCD FReLoN camera. Each image was azimuthally averaged and converted

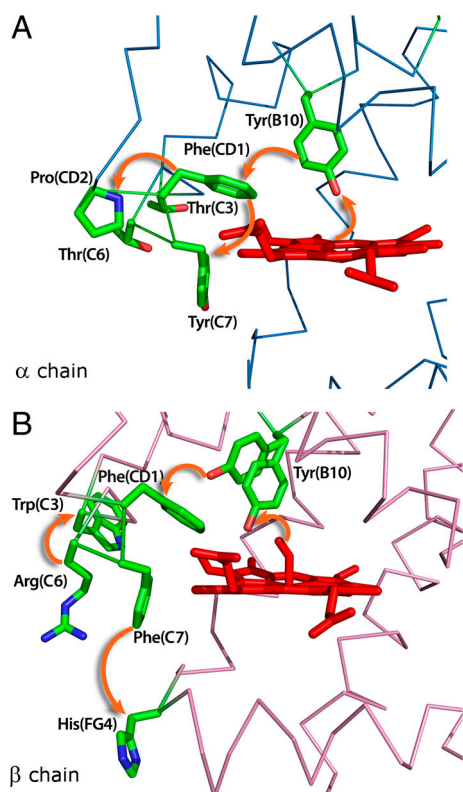


**Fig. 4.** Close-up view of T state HbYQ  $\alpha$  chain (A) and  $\beta$  chain (B) in the proximity of the heme; notice that CO is bound to the  $\beta$  chains only. The contacts that could allow distal tertiary changes to be transmitted from the heme pocket to the hinge and the switch regions of the  $\alpha_1\beta_2$  interface are indicated by orange arrows.

into a one-dimensional q-curve using a wavelength of 0.6793 Å corresponding to the peak of the X-ray spectrum. After normalization (in the 2–2.2 Å<sup>-1</sup> q-region), a reference scattering pattern (“laser off” image), which probed the unexcited sample, was subtracted from the scattering pattern at a given time delay (“laser on” image). Difference patterns at the same time delay were averaged. Structural changes occurring at different time delays leave their “fingerprints” in the “laser on—laser off” differences.

**MWC Allosteric Kinetic Model.** The kinetic model used to analyze the TR-WAXS difference patterns is similar to that originally introduced by Sawicki and Gibson (2). It assumes Hb to populate two quaternary conformations, R and T, and five ligation states (R<sub>i</sub> and T<sub>i</sub>, where *i* = 0–4). A single bimolecular ligand-rebinding rate constant (apart from statistical factors) is introduced in the model for each quaternary state (the microscopic bimolecular association rates being indicated as <sup>R</sup>k<sub>on</sub> and <sup>T</sup>k<sub>on</sub>, respectively). It is well established (32) that, in the case of CO binding, cooperativity is fully expressed in the association rate constants; since the dissociation rate constants (<sup>R</sup>k<sub>off</sub> and

<sup>T</sup>k<sub>off</sub>) are not only independent of state, but are also extremely small, they have been neglected in the model. The R<sub>i</sub>–T<sub>i</sub> transition rates are assumed to be proportional to the R<sub>0</sub>–T<sub>0</sub> one and to scale down with the number of ligands bound through the parameter *s* (2, 23). The reverse T–R transition rates are linked to the forward R–T rates through thermodynamic equilibrium relations that make use of the allosteric constant L<sub>0</sub> = [T<sub>0</sub>]/[R<sub>0</sub>] and the affinity ratio *c* = <sup>T</sup>K/<sup>R</sup>K, where <sup>T</sup>K and <sup>R</sup>K are the equilibrium association constants to the T and R states, respectively.

Further details on sample preparation and handling, data refinement, and best fit of the data in terms of the MWC kinetic model are given in *SI Materials and Methods*.

**ACKNOWLEDGMENTS.** We thank Prof. A. Bellelli for further analysis of the already published O<sub>2</sub> equilibrium data on HbYQ and M. Wulff for assistance during the experiments. This work was supported by the Italian MIUR Grant PRIN 2008 to A.C. (Prot. 2008ZWHZJT) and FIRB Proteomica 2007 to M.B. (Prot. RBRN07BMCT).

- Monod J, Wyman J, Changeux JP (1965) On the nature of allosteric transitions: A plausible model. *J Mol Biol* 12:88–118.
- Sawicki CA, Gibson QH (1976) Quaternary conformational changes in human hemoglobin studied by laser photolysis of carboxyhemoglobin. *J Biol Chem* 251:1533–1542.
- Hofrichter J, Sommer JH, Henry ER, Eaton WA (1983) Nanosecond absorption spectroscopy of hemoglobin: Elementary processes in kinetic cooperativity. *Proc Natl Acad Sci USA* 80:2235–2239.
- Friedman JM (1985) Structure, dynamics, and reactivity in hemoglobin. *Science* 228:1273–1280.
- Rodgers KR, Spiro TG (1994) Nanosecond dynamics of the R → T transition in hemoglobin: Ultraviolet Raman studies. *Science* 265:1697–1699.
- Eaton WA, et al. (2007) Evolution of allosteric models for hemoglobin. *IUBMB Life* 59:586–599.
- Sawicki CA, Gibson QH (1977) Quaternary conformational changes in human oxyhemoglobin studied by laser photolysis. *J Biol Chem* 252:5783–5788.
- Perutz MF (1970) Stereochemistry of cooperative effects in haemoglobin. *Nature* 228:726–739.
- Baldwin J, Chothia C (1979) Haemoglobin: The structural changes related to ligand binding and its allosteric mechanism. *J Mol Biol* 129:175–220.
- Balakrishnan G, et al. (2004) Time-resolved absorption and UV resonance Raman spectra reveal stepwise formation of T quaternary contacts in the allosteric pathway of hemoglobin. *J Mol Biol* 340:843–856.
- Goldbeck RA, Esquerra RM, Kliger DS (2002) Hydrogen bonding to Trp β37 is the first step in a compound pathway for hemoglobin allostery. *J Am Chem Soc* 124:7646–7647.
- Cammarata M, et al. (2008) Tracking the structural dynamics of proteins in solution using time-resolved wide-angle X-ray scattering. *Nat Methods* 5:881–886.
- Cammarata M, Levantino M, Wulff M, Cupane A (2010) Unveiling the timescale of the R-T transition in human hemoglobin. *J Mol Biol* 400:951–962.
- Fischer S, Olsen KW, Nam K, Karplus M (2011) Unsuspected pathway of the allosteric transition in hemoglobin. *Proc Natl Acad Sci USA* 108:5608–5613.
- Miele AE, et al. (1999) Modulation of ligand binding in engineered human hemoglobin distal pocket. *J Mol Biol* 290:515–524.
- Miele AE, Draghi F, Vallone B, Boffi A (2002) The carbon monoxide derivative of human hemoglobin carrying the double mutation LeuB10 → Tyr and HisE7 → Gln on α and β chains probed by infrared spectroscopy. *Arch Biochem Biophys* 402:59–64.
- Miele AE, et al. (2001) Control of heme reactivity by diffusion: Structural basis and functional characterization in hemoglobin mutants. *Biochemistry* 40:14449–14458.
- Bourgeois D, et al. (2003) Complex landscape of protein structural dynamics unveiled by nanosecond Laue crystallography. *Proc Natl Acad Sci USA* 100:8704–8709.
- Brunori M, et al. (1999) Structural dynamics of ligand diffusion in the protein matrix: A study on a new myoglobin mutant Y(B10) Q(E7) R(E10). *Biophys J* 76:1259–1269.
- Cho HS, et al. (2010) Protein structural dynamics in solution unveiled via 100-ps time-resolved x-ray scattering. *Proc Natl Acad Sci USA* 107:7281–7286.
- Henry ER, Bettati S, Hofrichter J, Eaton WA (2002) A tertiary two-state allosteric model for hemoglobin. *Biophys Chem* 98:149–164.
- Henry ER, Jones CM, Hofrichter J, Eaton WA (1997) Can a two-state MWC allosteric model explain hemoglobin kinetics? *Biochemistry* 36:6511–6528.
- Jones CM, et al. (1992) Speed of intersubunit communication in proteins. *Biochemistry* 31:6692–6702.
- Perrella M, Colosimo A, Benazzi L, Ripamonti M, Rossi-Bernardi L (1990) What the intermediate compounds in ligand binding to hemoglobin tell about the mechanism of cooperativity. *Biophys Chem* 37:211–223.
- Perrella M, Di Cera E (1999) CO ligation intermediates and the mechanism of hemoglobin cooperativity. *J Biol Chem* 274:2605–2608.
- Goldbeck RA, Paquette SJ, Bjorling SC, Kliger DS (1996) Allosteric intermediates in hemoglobin. 2. Kinetic modeling of HbCO photolysis. *Biochemistry* 35:8628–8639.
- Edelstein SJ, Changeux JP (2010) Relationships between structural dynamics and functional kinetics in oligomeric membrane receptors. *Biophys J* 98:2045–2052.
- Perutz MF, Fermi G, Luisi B, Shaanan B, Liddington RC (1987) Stereochemistry of cooperative mechanisms in hemoglobin. *Acc Chem Res* 20:309–321.
- Park SY, Yokoyama T, Shibayama N, Shiro Y, Tame JR (2006) 1.25 Å resolution crystal structures of human haemoglobin in the oxy, deoxy and carbonmonoxy forms. *J Mol Biol* 360:690–701.
- Savino C, et al. (2009) Pattern of cavities in globins: The case of human hemoglobin. *Biopolymers* 91:1097–1107.
- Levantino M, Cupane A, Zimanyi L (2003) Quaternary structure dependence of kinetic hole burning and conformational substates interconversion in hemoglobin. *Biochemistry* 42:4499–4505.
- Antonini E, Brunori M (1971) *Hemoglobin and Myoglobin in their Reactions with Ligands* (North-Holland, Amsterdam).

# Supporting Information

Levantino et al. 10.1073/pnas.1205809109

## SI Text

**SI Discussion. Absence of geminate rebinding in HbYQ.** We have compared the structure of deoxy HbYQ, which is in T state (1), with the structure of the photolytic intermediate of R state HbA where, after partial photolysis, CO is found in the distal heme pocket above pyrrole ring C at about 3.5 Å from the iron in both  $\alpha$  and  $\beta$  chains (2). In HbYQ, the substitution Leu(B10)  $\rightarrow$  Tyr introduces additional bulk on top of the C pyrrole, thus obliterating this docking site for photolyzed CO. By superimposing the structure of the photolytic intermediate of partially ligated, cross-linked hybrids of T state HbA (2) with the  $\alpha$  and  $\beta$  chains of HbYQ we observed that the distance between photolyzed CO and Tyr(B10) is such that also in the T state the primary docking site is partially obliterated (CO is at distance of 0.86 Å from Tyr(B10) hydroxyl group and 1.23 Å from CZ of Tyr(B10) aromatic ring). In T state HbA chains, a second docking site for photolyzed CO was detected in the  $\beta$  chains, surrounded by Leu(B10), Val(E11), Leu(E12) and Leu(G8); the accessibility of this hydrophobic cavity is reduced by mutation Leu(B10)  $\rightarrow$  Tyr, as confirmed by the reduced occupancy of Xe in HbYQ (3).

**Preferential binding of CO to  $\beta$  chains of HbYQ and its consequences on the tertiary transition.** Crystallographic and functional data (1, 4) indicate that in HbYQ ligand binding occurs preferentially to the  $\beta$  chains and that it may be associated to late or reduced  $\beta$  chains tertiary transition impairing transmission of the binding event from tertiary to quaternary rearrangements. By comparing the distances of Tyr(B10) and Gln(E7) from the heme iron in  $\alpha$  and  $\beta$  chains we can conclude that the heme is more accessible for binding in the latter (distances from the iron: 3.85 Å and 3.95 Å in  $\alpha$  chains vs. 4.21 Å and 4.67 Å in  $\beta$  chains) (Fig. S1B and D). As we compared the structures of deoxy T state HbA (5) with HbYQ (3) we observed that the introduction of Tyr(B10) and Gln(E7) is associated with significant steric hindrance to ligand binding in the  $\alpha$  chains as compared to HbA (Fig. S1A): the NE atom of Gln(E7) is 0.5 Å closer to the heme with respect to distal HisE7 and its position is fixed by an interaction with Tyr(B10), which is also located on top of the heme at a short distance from the iron (3.85 Å). Moreover the hydroxyl group from Tyr(B10) occupies the position of the water molecule loosely bound to deoxy HbA  $\alpha$  chains upon which ligand binding is displaced; clearly in the mutant the whole tyrosine side chain has to move away to allow space for ligand binding. On the other hand, comparison of binding sites in  $\beta$  chains (Fig S1B) shows that in HbYQ, Gln(E7) coincides with the position occupied by His(E7) in HbA and the hydroxyl group of Tyr(B10) is at 4.67 Å from the heme iron.

To evaluate the steric availability for ligation of the iron of mutated chains we have also overlaid the chains of HbA in the deoxy and CO-bound states onto those of deoxy HbYQ by using the heme as a reference (Fig. S2). In HbA  $\alpha$  chains the ligand is accommodated by a 0.9 Å displacement of His(E7) and water expulsion, whereas in the  $\alpha$  chains of HbYQ, Tyr(B10) and Gln(E7) would pose a more severe hindrance to the approach of a ligand. We observed that in mutated  $\beta$  chains the distal site allows more space on top of the heme iron with respect to  $\alpha$  chains; indeed, the distance of CO bound to the heme from Tyr(B10) and Gln(E7) would be 1.36 Å and 2.01 Å in  $\alpha$  chains (Fig. S2B) and 2.50 Å and 2.72 Å in  $\beta$  chains (Fig. S2D). On the other hand, in HbA there seems to be no major difference in the hindrance of binding between the two types of chains, in agreement with

experimental data (Fig. S2A and C) (6). In conclusion, the introduction of a tyrosine in B10 and of a glutamine in E7 seems to lead to preferential binding of ligands to  $\beta$  chains, and in both chains an additional barrier to ligand diffusion is present, accounting for low affinity.

In order to shed light on the structural basis for the late switch-over point of HbYQ we carried out further analysis of available structures to single out the effect of the mutations on the tertiary transition. M. Perutz predicted that Val67(E11) would pose steric hindrance to ligand binding only in the  $\beta$  chains due to vicinity to ligands onto the heme iron (7). The analysis by Baldwin and Chothia (8) confirmed that in the  $\beta$  chains ligand binding is accompanied by a 1.5 Å shift of the heme towards the interior of the protein, whereas in the  $\alpha$  chains it amounts to only 0.6 Å. This heme displacement eliminates the steric interference of distal Val67(E11) with bound ligands in  $\beta$  chains, therefore upon binding this residue is not displaced, but the heme gets more deeply buried in the protein matrix. As observed by the analysis of the high-resolution structures of HbA and those of partially or fully ligated derivatives of T state HbA (5, 9–11), in the  $\beta$  chains the displacement of the iron upon binding is of a smaller extent than what observed in the  $\alpha$  chains, the tertiary rearrangement being driven mainly by the heme displacement that pulls the proximal His92(F8), and F and G helices. We therefore analyzed the structures of HbYQ in order to understand the effect of the mutations on the tertiary transition triggered by ligand binding, taking into account proximal and distal control of ligand binding in the  $\alpha$  and  $\beta$  Hb chains, respectively. In crystals of deoxy (T state) HbYQ, CO binds only to  $\beta$  chains (4) as shown in Fig. S3. In the  $\beta_2$  chain CO is accommodated with a slight displacement of Tyr(B10) and Gln(E7) (Fig. S3A). The  $\beta_1$  chain, less constrained by crystal contacts, shows two conformations; one similar to the one adopted by  $\beta_2$  and another in which Gln(E7) moves towards the bulk (not shown) while Tyr(B10) swings away from the ligand (Fig. S3B). Val(E11) shows a modest displacement in both  $\beta_1$  and  $\beta_2$ , and the iron moves towards the plane in both  $\beta$  chains, pulling the proximal His with a small (about 0.3 Å) shift of the F helix. This structure shows that CO can be bound to HbYQ  $\beta$  chains in the T state with a very slight steric conflict; i.e. a distance of 2.50 Å from the OH group of Tyr(B10). This conformation may represent the first step of ligand binding to HbYQ. Nevertheless Tyr(B10) does not allow the shift of the heme characteristic of the R state, and the swung conformer adopted by Tyr(B10) in the  $\beta_1$  chains might represent a second step after binding, in which the presence of the ligand is felt at the distal side of the heme, and the tertiary change can take place. In other words, in both  $\beta$  chains, CO can bind without causing major tertiary rearrangements and the lattice forces prevail over quaternary transitions, at least over a time of several hours before the crystals are frozen for data collection. This is at variance with respect to high salt crystals of HbA that lose crystal order upon ligand binding.

**The  $R_0$ - $T_0$  allosteric transition.** Whereas the late switch-over point of HbYQ and its low affinity for ligands explain why the recovery of the  $R_4$  state is not yet complete after 1 s, the structural basis for the 10-fold decrease of the  $R_0 \rightarrow T_0$  transition is not evident, also because the structure of R state HbYQ is unfortunately not available. A recently published study by Fischer et al. (12) adopted a conjugate peak refinement algorithm to describe the path between the T and R states, identifying two sequential quaternary

transitions ( $Q_1$  and  $Q_2$ ). This simulation is supported by time-resolved UVRR spectroscopy (13) showing a fast and a slow phase (2  $\mu$ s and 20  $\mu$ s) for HbA quaternary transition and by TR-WAXS that detects a fast signal for the quaternary transition of HbA (1–2  $\mu$ s) with the hypothesis of a slower phase, undetected due to a smaller structural extent. The signature of the fast component (2  $\mu$ s) of the quaternary transition corresponds to a specific UVRR spectroscopic signal (13) due to Trp37 in the  $\beta$  chains, located in the flexible joint region (involving the  $\beta$  C-helix and the  $\alpha$  FG-corner). The simulation described by Fisher et al. (12) placed the transition of Trp37(C3)  $\beta$  and the switch of His97 (FG4) $\beta$  in the main, fast phase of the quaternary transition. These two residues are located in the  $\alpha_1\beta_2$  interface, formed by the C helix and FG corner of both  $\alpha$  and  $\beta$  chains. The mutations introduced in HbYQ are located on the distal side of the heme and we have attempted to single out how they can affect the  $\alpha_1\beta_2$  interface, where the quaternary transition is associated with clear-cut changes. Fig. 4 in the main text shows that substitution Leu(B10)  $\rightarrow$  Tyr can affect the CD corner and the C helix (residues 42–49 and 35–41 in the  $\beta$  chains and 43–49 and 36–42 in the  $\alpha$  chains) through a network of contacts, as highlighted by the arrows (upper right). The swinging of Tyr(B10) that occurs upon CO binding induces a contact with Phe(CD1) $\beta$  in the CD corner, contrasting its slight upwards movement due to the heme shift (Fig. 4B). This pressure can be transmitted and amplified to Trp37(C3)  $\beta$  via Phe41(C7)  $\beta$  and preceding residues. Fig. 4A shows that Pro44(CD3), Thr41(C6), and Thr38(C3) in  $\alpha$  chains could be also affected by the dynamics of Tyr(B10), similarly to the  $\beta$  chains, via Phe43(CD1) and Tyr42(C7). This network of contacts would allow distal tertiary changes to be transmitted at the level of the flexible joint and the switch of the  $\alpha_1\beta_2$  interface. We may therefore hypothesize that in HbYQ, where Tyr (B10) has to rearrange upon ligand binding, the barrier to cross to achieve the quaternary transition is higher, leading to a decrease in the  $R_0 \rightarrow T_0$  transition rate. In HbA, comparison of the contacts of Trp37 $\beta$  in the deoxy (T) and in the CO (R) states shows a rearrangement of this residue (14), which can be affected by Tyr(B10) through the contacts described above. Fig. S6 shows the rearrangement of the environment of this residue due to the quaternary transition in the  $\alpha_1\beta_2$  interface.

**SI Materials and Methods. Sample preparation and handling.** HbA was purified from freshly collected human blood with standard techniques (15) while the HbYQ mutant was expressed in *E. coli* and purified to homogeneity as previously reported (1). All experiments were carried out in a 0.1 M phosphate buffer at neutral pH and 20 °C unless otherwise specified. Organic phosphates that strongly affect the R-T equilibrium, such as 1,2-diphosphoglycerate, were stripped from Hb molecules. All reagents were of analytical grade. Hb samples to be used for TR-WAXS experiments were equilibrated for approximately 20 min with humidified CO. A small amount of a CO-saturated Na-dithionite solution was added anaerobically to ensure full reduction of the iron. The final Na-dithionite concentration was 8 mM in all samples. The HbA samples were 4 mM (in heme) while the HbYQ were 2 mM (in heme). Approximately 100  $\mu$ l of a freshly prepared CO-saturated Hb solution was loaded in a 2 mm diameter quartz capillary (Hilgenberg GmbH). Two CO bubbles were trapped on both sides of the protein solution volume. A CO-saturated glycerol drop prevented gas leakage at the open side of the capillary. All capillaries were further sealed with capillary wax (Hampton Research) and nail varnish.

**Subtraction of the heating contribution.** Laser-induced X-ray scattering differences contain not only fingerprints of protein structural changes but also solvent heating contributions arising from

changes in solvent temperature, density, and pressure that are induced by the energy transferred from the laser into the solvent via protein absorption (16, 17). To decouple the two contributions, we have collected TR-WAXS data on cyanomet-hemoglobin (HbCN) in the same experimental conditions used for the other samples. HbCN has a molar extinction coefficient at 532 nm close to that of HbCO, whereas the bond between the CN<sup>-</sup> ion and the iron cannot be photolyzed. As the sample is photoexcited by the laser pulse, the delivered energy does not induce any conformational change on the protein. All the energy is delivered to the solvent, inducing a temporary heating of the solution (associated to a structural rearrangement of the solvent molecules). Scattering difference patterns of an HbCN sample are thus a measure of the solvent heating contribution. In order to isolate the protein contribution in the TR-WAXS difference patterns, we have subtracted from the pattern measured at a given time delay the pattern of the HbCN sample at the same time delay.

**Singular value decomposition.** The number of structurally distinguishable signals contained in the TR-WAXS patterns collected at time delays longer than 250 ns has been estimated through singular value decomposition (SVD). Judging from the magnitude of the singular values, the signal-to-noise ratios, and the autocorrelations of each SVD component, we concluded that only the first two SVD components are significant in the case of both HbA and HbYQ data. A check of this assumption has been obtained by verifying, for both sets of data, that a good quality reconstruction of the experimental patterns is indeed obtained, at all time delays, if only the first two SVD components are kept.

**Kinetic model and fit.** The kinetic model used to fit our TR-WAXS data (see Fig. S4) corresponds to a set of differential equations describing how the population of the different molecular species of the system evolves with time. The model, similar to that originally introduced by Sawicki and Gibson (18) and already successfully used for TR-WAXS data analysis on Hb solutions (16, 17), assumes the presence of Hb molecules in two quaternary conformations, R and T, and five ligation states ( $R_i$  and  $T_i$ , where  $i = 0$  to 4) indicates the number of bound ligands. A single bimolecular ligand-rebinding rate constant (apart from statistical factors) is introduced in the model for each quaternary state (the microscopic bimolecular rates to R and T states indicated as  ${}^Rk_{\text{on}}$  and  ${}^Tk_{\text{on}}$ , respectively). It is well established (19) that, in the case of CO binding, cooperativity is fully expressed in the association rate constants; since the dissociation rate constants ( ${}^Rk_{\text{off}}$  and  ${}^Tk_{\text{off}}$ ) are not only independent of state, but are extremely small, they have been neglected in the model. The complete set of R–T transition rates are assumed to be proportional to the  $R_0$ – $T_0$  transition rate and to scale down with the number of bound ligands through the  $s$  parameter (20). The inverse T–R transition rate are linked to the direct R–T rates through thermodynamic equilibrium relations that make use of the allosteric constant  $L_0 = [T_0]/[R_0]$  and the affinity ratio  $c = {}^Tk_{\text{off}}/{}^Rk_{\text{off}}$ , where  ${}^TK$  and  ${}^RK$  are the equilibrium association constants to the T and R states, respectively. The set of differential equations associated with this kinetic model (one for each Hb microscopic state plus one that describes the time evolution of the unbound CO concentration) have been solved under the following initial conditions:

$$\begin{aligned}
 [T_i] &= 0 \quad \text{for } i = 0, \dots, 4 \\
 [R_i] &= [Hb] \binom{4}{i} (1 - N_0)^i N_0^{4-i}, \quad \text{[S1]}
 \end{aligned}$$

where  $N_0$  is the fraction of deoxy hemes at 250 ns from photolysis. The choice of the  $R_i$  initial populations is justified by the assumption that each photolysis event is uncorrelated with the previous photolysis of a heme-CO complex of the same Hb tetramer. In this hypothesis, the distribution of  $R_i$  ligated species is given by the above binomial distribution. The kinetic model has seven independent parameters ( $N_0$ ,  $k_0$ ,  $s$ ,  $L_0$ ,  $c$ ,  ${}^Rk_{on}$ , and  ${}^Tk_{on}$ ). In order to reduce the number of fitting parameters,  ${}^Rk_{on}$  and  ${}^Tk_{on}$  have been fixed to the values obtained from partial photolysis and rapid mixing measurements, respectively (1, 4). In view of the SVD result, the measured TR-WAXS patterns,  $\Delta S(q, t)$ , have been decomposed in terms of two basis patterns,  $\Delta S_{R-like}(q)$  and  $\Delta S_{T-like}(q)$ , that represent, respectively, the effect of tertiary relaxations that have occurred in  $R_i$  states within 250 ns from photolysis, and that of the R-T quaternary transition:

$$\Delta S(q, t) = R\text{-like}(t) \times \Delta S_{R-like}(q) + T\text{-like}(t) \times \Delta S_{T-like}(q), \quad [S2]$$

where R-like(t) and T-like(t) are weighted sum of the  $R_i(t)$  and

$T_i(t)$  populations:

$$T\text{-like}(t) = \frac{1}{[Hb]} ([T_0](t) + [T_1](t) + [T_2](t) + [T_3](t) + [T_4](t))$$

$$R\text{-like}(t) = \frac{1}{[Hb]} \left( [R_0](t) + \frac{3}{4}[R_1](t) + \frac{1}{2}[R_2](t) + \frac{1}{4}[R_3](t) \right). \quad [S3]$$

The kinetic parameters featuring in the model and the  $\Delta S_{R-like}(q)$  and  $\Delta S_{T-like}(q)$  basis patterns have been fitted against the experimental TR-WAXS patterns with an approach analogous to that used for analyzing time-resolved spectroscopic data (21, 22). The idea of this approach is to add a priori information on kinetics to obtain a minimal set of q-patterns (basis patterns) that are able to reproduce the data and, at the same time, have a clear physical meaning. The results of the fitting procedure are illustrated in Fig. 1 of the main text. Best-fit values and parameters errors reported in Table 1 have been estimated using the Minuit minimization algorithm and the Minuit processor MINOS (23).

- Miele AE, et al. (1999) Modulation of ligand binding in engineered human hemoglobin distal pocket. *J Mol Biol* 290:515–524.
- Adachi S, Park SY, Tame JR, Shiro Y, Shibayama N (2003) Direct observation of photolysis-induced tertiary structural changes in hemoglobin. *Proc Natl Acad Sci USA* 100:7039–44.
- Savino C, et al. (2009) Pattern of cavities in globins: The case of human hemoglobin. *Biopolymers* 91:1097–1107.
- Miele AE, et al. (2001) Control of heme reactivity by diffusion: Structural basis and functional characterization in hemoglobin mutants. *Biochemistry* 40:14449–14458.
- Park SY, Yokoyama T, Shibayama N, Shiro Y, Tame JR (2006) 1.25 Å resolution crystal structures of human haemoglobin in the oxy, deoxy and carbonmonoxy forms. *J Mol Biol* 360:690–701.
- Perrella M, Di Cera E (1999) CO ligation intermediates and the mechanism of hemoglobin cooperativity. *J Biol Chem* 274:2605–2608.
- Perutz MF (1970) Stereochemistry of cooperative effects in haemoglobin. *Nature* 28:726–739.
- Baldwin J, Chothia C (1979) Haemoglobin: the structural changes related to ligand binding and its allosteric mechanism. *J Mol Biol* 129:175–220.
- Park SY, Shibayama N, Hiraki T, Tame JRH (2004) Crystal structures of unliganded and half-liganded human hemoglobin derivatives cross-linked between Lys 82 $\beta_1$  and Lys 82 $\beta_2$ . *Biochemistry* 43:8711–8717.
- Mozzarelli A, Rivetti C, Rossi GL, Eaton WA, Henry ER (1997) Allosteric effectors do not alter the oxygen affinity of hemoglobin crystals. *Protein Sci* 6:484–489.
- Paoli M, Liddington R, Tame J, Wilkinson A, Dodson G (1996) Crystal structure of Tstate haemoglobin with oxygen bound at all four haems. *J Mol Biol* 256:775–792.
- Fischer S, Olsen KW, Nam K, Karplus M (2011) Unsuspected pathway of the allosteric transition in hemoglobin. *Proc Natl Acad Sci USA* 108:5608–5613.
- Balakrishnan G, et al. (2004) Time-resolved absorption and UV resonance Raman spectra reveal stepwise formation of T quaternary contacts in the allosteric pathway of hemoglobin. *J Mol Biol* 340:843–856.
- Vallone B, Bellelli A, Miele AE, Brunori M, Fermi G (1996) Probing the  $\alpha_1\beta_2$  interface of human hemoglobin by mutagenesis. Role of the FG-C contact regions. *J Biol Chem* 271:12472–12480.
- Levantino M, Cupane A, Zimanyi L (2003). Quaternary structure dependence of kinetic hole burning and conformational substates interconversion in hemoglobin. *Biochemistry* 42:4499–4505.
- Cammarata M, et al. (2008) Tracking the structural dynamics of proteins in solution using time-resolved wide-angle X-ray scattering. *Nat Methods* 5:881–886.
- Cammarata M, Levantino M, Wulff M, Cupane A (2010) Unveiling the timescale of the R-T transition in human hemoglobin. *J Mol Biol* 400:951–962.
- Sawicki CA, Gibson QH (1976) Quaternary conformational changes in human hemoglobin studied by laser photolysis of carboxyhemoglobin. *J Biol Chem* 251:1533–1542.
- Antonini E, Brunori M (1971) *Hemoglobin and Myoglobin in Their Reactions with Ligands* (North-Holland, Amsterdam).
- Jones CM, et al. (1992) Speed of intersubunit communication in proteins. *Biochemistry* 31:6692–6702.
- Henry ER, Jones CM, Hofrichter J, Eaton WA (1997) Can a two-state MWC allosteric model explain hemoglobin kinetics? *Biochemistry* 36:6511–6528.
- Henry ER, Bettati S, Hofrichter J, Eaton WA (2002) A tertiary two-state allosteric model for hemoglobin. *Biophys Chem* 98:149–164.
- James F, Roos M (1975) Minuit: A system for function minimization and analysis of the parameters errors and correlations. *Comput Phys Commun* 10:343–367.





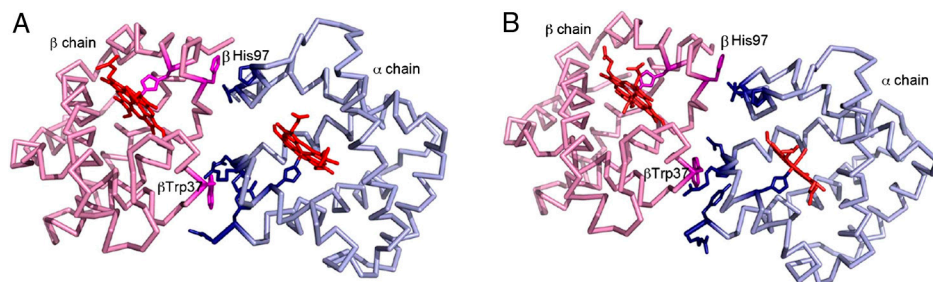


**Fig. 56.** The  $\alpha_1\beta_2$  interface in deoxy (A) and CO-bound (B) HbA.  $\alpha$  chains are drawn in blue and  $\beta$  chains in purple. The amino acids contacting  $\beta$ His97 and  $\beta$ Trp37 are shown. The orientation of the  $\beta$  chain was left unchanged in the picture in order to facilitate the comparison of intermolecular contacts upon the quaternary transition.